
Forging Time Series with Language: A Large Language Model Approach to Synthetic Data Generation

Cécile Rousseau
IBM Research Europe
rousseau.cecile@ibm.com

Tobia Boschi
IBM Research Europe
tobia.boschi@ibm.com

Giandomenico Cornacchia
IBM Research Europe
Giandomenico.Cornacchia1@ibm.com

Dhaval Salwala
IBM Research Europe
dhaval.vinodbhai.salwala@ibm.com

Alessandra Pascale
IBM Research Europe
apascale@ie.ibm.com

Juan Bernabe Moreno
IBM Research Europe
juan.bernabe-moreno@ibm.com

Abstract

SDForger is a flexible and efficient framework for generating high-quality multivariate time series using LLMs. Leveraging a compact data representation, SDForger provides synthetic time series generation from a few samples and low-computation fine-tuning of any autoregressive LLM. Specifically, the framework transforms univariate and multivariate signals into tabular embeddings, which are then encoded into text and used to fine-tune the LLM. At inference, new textual embeddings are sampled and decoded into synthetic time series that retain the original data’s statistical properties and temporal dynamics. Across a diverse range of datasets, SDForger outperforms existing generative models in many scenarios, both in similarity-based evaluations and downstream forecasting tasks. By enabling textual conditioning in the generation process, SDForger paves the way for multimodal modeling and the streamlined integration of time series with textual information. The model is open-sourced at https://github.com/IBM/fms-dgt/tree/main/fms_dgt/public/databuilders/time_series.

1 Introduction

In the era of foundation models, integrating time-series analysis with language models (LLMs) has emerged as a key research priority, spurring work on specialized models for forecasting, anomaly detection and root cause analysis (Liang et al., 2024). These efforts aim to harness the representational power of LLMs to tackle complex temporal dependencies. Despite these advancements, foundation models for time series still struggle with concept drift, high variability, and face performance degradation over long horizons. In addition, the scarcity of large and diverse time-series datasets often limits model generalization, especially in domains where data collection is expensive or operationally constrained, such as climate science, finance, or plasma physics (Kit et al., 2024).

In this context, *synthetic data generation has emerged as a complementary research direction to improve scalability and model performance, particularly in low-quality or data-scarce settings*. In particular, synthetic data can be leveraged to fine-tune machine learning models on domain-specific distributions, reducing the need to train models from scratch and improving sample efficiency. Indeed,

several generative models for time series have been proposed, including VAE-based architectures (Desai et al., 2021; Lee et al., 2023), GANs (Pei et al., 2021; Kidger et al., 2021), and diffusion-based approaches (Zhou et al., 2023). While these methods have shown promise, they typically lack pre-training, require task-specific retraining, and often struggle with long-term dependencies, multivariate coupling, and distributional shifts (Ang et al., 2023).

Recent studies have instead explored the use of LLMs for synthetic tabular data generation (Padhi et al., 2021; Borisov et al., 2022), demonstrating that language models trained on text-encoded data can capture statistical relationships and feature dependencies effectively. However, extending these methods to time series is non-trivial: long temporal windows increase inference and training costs, while temporal and multivariate correlations require more structured modeling.

These limitations highlight the need for novel methodologies that adapt LLMs for time-series generation while addressing temporal, structural, and computational challenges. We introduce **SDForger** (Synthetic Data Forger), a novel framework for generating high-quality *univariate and multivariate time series*, even in data-scarce settings. SDForger leverages foundation models with minimal fine-tuning by operating over compact tabular embeddings derived from functional decompositions.

Key features and advantages of SDForger:

- **Compact basis representation** SDForger uses FastICA or PCA to embed time series into low-dimensional tabular data. These capture key temporal and inter-variable structures while decoupling the embedding from sequence length, enabling efficient processing of long signals.
- **Text-to-sequence generation via LLMs** The embedding tables are converted into structured textual prompts and used to fine-tune a language model. A guided inference approach is then used to generate structured embeddings, ensuring that the synthetic data retains the original dataset’s statistical properties and feature relationships.
- **Flexible, lightweight architecture** The framework leverages autoregressive LLMs, including lightweight models, and requires only a small number of training instances. Its modular design enables easy adaptation to different generation tasks and architectures, while its compact embedding space ensures fast inference, even for long time-series windows.
- **Multivariate and multimodal readiness** SDForger can model complex multivariate dynamics and supports future extensions to textual conditioning, enabling generation guided by both time-series structure and external language-based context.

By combining structured embeddings with LLM-based generation, SDForger establishes a new paradigm for scalable, interpretable, and high-quality synthetic time-series generation.

Our simulations demonstrate that SDForger not only generates statistically realistic time series but also improves downstream model performance, often matching or exceeding results obtained from real data alone. This is particularly valuable in practical scenarios where access to high-quality data is limited or where distribution shifts make original training data less effective. Compared to state-of-the-art generative models, SDForger achieves competitive or superior performance across a wide range of similarity metrics and utility-based evaluations. Notably, our experiments show that even lightweight, pretrained LLMs (e.g., GPT-2) are sufficient to produce high-quality synthetic data with minimal fine-tuning, highlighting the accessibility, efficiency, and flexibility of our approach.

In the remainder of this paper, we first review related work (Section 2), then detail the SDForger framework (Section 3), describe our evaluation setup (Section 4), present extensive experimental results (Section 5), highlight the flexibility of language models (Section 6), and conclude with key takeaways and future directions (Section 7).

2 Related work

Time-series generation Recent advances in time-series generation have introduced a variety of deep generative models, including GAN-based approaches like TimeGAN (Smith and Smith, 2020), state-space models, and vector-quantized architectures such as TimeVQVAE (Lee et al., 2023). While these methods generate realistic sequences, they often struggle with multivariate dependencies, and require training from scratch for each dataset. More recent frameworks integrate randomly-weighted combinations of time series to improve their pretraining pipeline, e.g. Chronos (Ansari et al., 2024) adapting the Mixup (Zhou et al., 2023) methodology for time series. To address evaluation challenges, TSGBench (Ang et al., 2023) proposes a unified benchmark of similarity, fidelity, and utility metrics.

Foundation models and LLMs for time series Recent advances have introduced foundation models specifically designed for time-series tasks, offering unified frameworks for forecasting, classification, and anomaly detection (Liang et al., 2024). Examples include TFT (Lim et al., 2021), TimeGPT (Garza and Mergenthaler-Canseco, 2023), and Chronos (Ansari et al., 2024), while lightweight models like TTMs (Ekambaram et al., 2024) focus on efficient multivariate forecasting. Parallel efforts have explored adapting LLMs to time-series data by encoding numerical sequences as text (Gruver et al., 2024; Zhou et al., 2023; Jin et al., 2023), enabling zero-shot inference and transfer learning. Notably, LLMTime (Gruver et al., 2024) and GPT4TS (Zhou et al., 2023) retain most of the LLM architecture while fine-tuning only shallow layers, and Time-LLM (Jin et al., 2023) employs reprogramming to adapt to temporal tasks. Despite these innovations, most existing approaches either require task-specific pretraining or struggle to model complex structures and may benefit from synthetic data for improving generalization and robustness.

Specialized architectures for time-series generation Several architectures have been specifically designed to capture temporal and multivariate dependencies in time series. Variational autoencoders such as TimeVAE (Desai et al., 2021) and TimeVQVAE (Lee et al., 2023) use recurrent or vector-quantized structures to model sequential dynamics. GAN-based approaches, including RTSGAN (Pei et al., 2021), SDEGAN (Kidger et al., 2021), and COSCI-GAN (Seyfi et al., 2022), employ recurrent or component-wise disentangled generators to capture complex temporal patterns adversarially. Diffusion-based models, like LS4 (Zhou et al., 2023), generate sequences through learned reverse-time processes. These specialized architectures complement general-purpose time-series generation methods and provide valuable baselines for evaluating synthetic data. However, these architectures are trained from scratch and cannot leverage existing pre-trained language or foundation models, limiting their scalability and adaptability across domains.

3 Methodology

In this section, we present our methodology, illustrated in Figure 1. SDForger is divided into three macro-steps: (i) *Preprocessing and embedding* transform the time series into tabular data (i.e., steps 1 to 3 highlighted in purple); (ii) *Fine-tuning and Generation* fine-tune a pre-trained LLM and generate new embedding instances (i.e., step 4 highlighted in green); (iii) *Decoding* reconstruct the original time-series space from the generated embeddings (i.e., steps 5 and 6 highlighted in light blue).

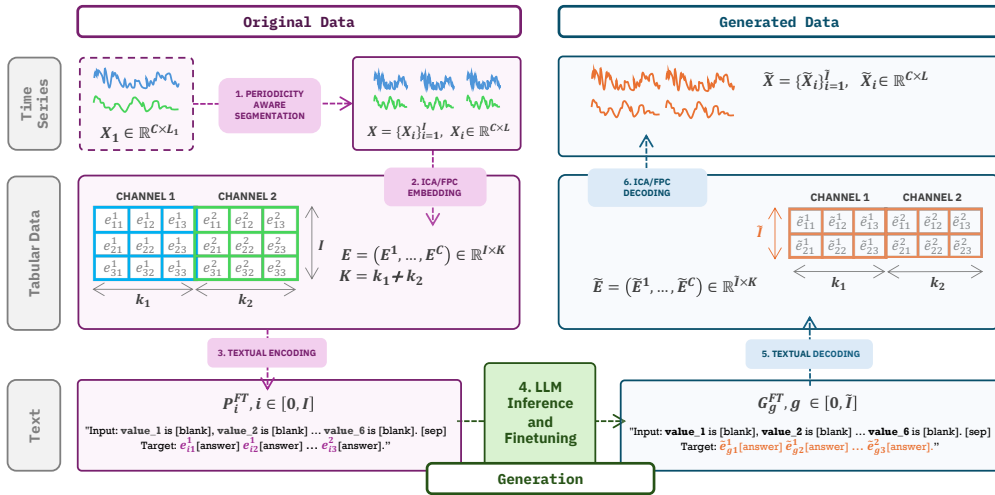


Figure 1: SDForger pipeline. Overview of the SDForger generation process. The example illustrates a setting with $I = 3$ input segments, $C = 2$ channels, $k_1 = k_2 = 3$ components, and $\bar{I} = 2$ generated samples. The model performs periodicity-aware segmentation, extracts embeddings, and embed them into text. An LLM is then fine-tuned to generate embedding sequences, which are finally decoded to reconstruct synthetic time series.

Notation Hereinafter, we introduce some basic notation. Let $X = \{X_i\}_{i=1}^I, X_i \in \mathbb{R}^{C \times L}$ represent a collection of I instances of a multivariate time series, where each instance has length L and consists

of C channels. The task of *synthetic time-series generation* can now be formally defined as producing \tilde{I} instances of a multivariate time series $\{\tilde{X}_i\}_{i=1}^{\tilde{I}}, \tilde{X}_i \in \mathbb{R}^{C \times L}$ conditioned on the given context X . Throughout the paper, we denote by $x_i^c \in \mathbb{R}^L$ the i -th instance of channel c , and by $X^c \in \mathbb{R}^{I \times L}$ the matrix collecting all instances associated with channel c .

Periodicity-aware segmentation In cases where only a single time series instance $X_1 \in \mathbb{R}^{C \times L_1}$ is available, we apply a segmentation strategy to artificially create multiple instances. The segmentation procedure facilitates the estimation of the time-series distribution. Specifically, we extract I periodicity-aware windows of fixed length $L < L_1$, aligning cuts with natural cycles and minimizing overlap to enhance independence and diversity. This pre-processing (described in Appendix A.1) transforms the data from a single sequence X_1 into a set $X = \{X_i\}_{i=1}^I$, where $X_i \in \mathbb{R}^{C \times L}$, preparing the data for the generation task.

3.1 From time series to tabular data

To enable tabular generation and analysis, SDForger transforms time series into structured tabular data using *basis decomposition techniques*. Each row represents a time series embedding obtained by projecting the signal onto a set of learned basis functions. Specifically, we adopt two decomposition methods: Functional Principal Components (FPC) (Ramsay and Silverman, 2005) and Fast Independent Component Analysis (FastICA) (Hyvarinen, 1999):

- **FPC** identifies principal modes of variation by performing eigen-decomposition of the covariance operator. It captures directions of maximal variance, preserving correlation across components, showing effectiveness in modeling multivariate longitudinal data (Boschi et al., 2024).
- **FastICA** extracts statistically independent components by maximizing non-Gaussianity. It decomposes a contrast function, uncovering independent latent factors that may not align with the directions of maximal variance.

Formally, for each channel c , we assume the instances (X_1^c, \dots, X_I^c) are realizations of continuous functions defined over $\mathcal{T} = [0, L]$. We approximate each X_i^c as a linear combination of k_c basis functions $(b_1^c, \dots, b_{k_c}^c)$, where the choice of basis depends on the decomposition method (non-Gaussianity-based for FastICA, covariance-based for FPC). The embedding coefficients are:

$$e_{ij}^c = \langle X_i^c, b_j^c \rangle_{\mathbb{L}^2} = \int_{\mathcal{T}} X_i^c(t) b_j^c(t) dt,$$

We define the embedding matrix for channel c , $E^c \in \mathbb{R}^{I \times k_c}$. By concatenating the embeddings across all channels, we obtain the final embedding table: $E = (E^1, \dots, E^C) \in \mathbb{R}^{I \times K}$ with $K = \sum_{c=1}^C k_c$.

Throughout this paper, we refer to the columns of E as embedding features. We denote the i -th row of E as E_i , corresponding to the embedding vector of instance X_i , and the value in its k -th column as e_{ik} . More details on the choice of k_c are given in Appendix A.2 and Appendix Table D.1.

Notably, both methods offer the advantage that their computational cost depends on the number of instances I and the number of components k_c , but not on the instance length L . This decoupling allows our algorithm to handle very long time windows without a corresponding increase in computational complexity, ensuring great flexibility and scalability.

3.2 Generation of tabular data

Our data generation block consists of three key stages: encoding tabular data into text, fine-tuning an LLM, and generating synthetic embeddings.

3.2.1 From embeddings table to text

LLMs are designed to process textual information. Therefore, applying an LLM to tabular data requires converting each row into a textual format that can serve as a prompt during the fine-tuning stage. Inspired by Donahue et al. (2020), we introduce a *Textual Encoder* responsible for converting tabular instances E_i into structured text representations using a Fill-In-The-Middle template.

Definition 1 (Textual encoder) Let $\mathcal{P}^{\text{FT}} = \{\mathcal{P}_i^{\text{FT}}\}_{i=1}^I$ denote the set of fine-tuning prompts, where:

$$\mathcal{P}_i^{\text{FT}} = \text{“Input: } \bigcirc_{k=1}^K (\text{value}_{\pi(k)} \text{ is [blank],) [sep]} \\ \text{Target: } \bigcirc_{k=1}^K (e_{i\pi(k)} \text{ [answer])”}$$

Here, the operator \bigcirc denotes the concatenation and π is a random permutation of K elements.

Random Feature Order Permutation. Encoding tabular data into text can introduce unintended positional biases, as LLMs inherently process tokens in sequence. To enforce order independence (Borisov et al., 2022), we apply a random permutation π to the encoded feature-value pairs within each instance. This shuffling ensures that the model does not infer any spurious relationships based on the ordering of features within the textual representation. For $K = 2$, an admissible finetuning prompt for E_i is: “Input: value_2 is [blank], value_1 is [blank] [sep] Target: e_{i2} [answer] e_{i1} [answer]”

3.2.2 Large language model finetuning and inference

Fine-tuning By training an LLM on structured text representations of the embedding tables, we enable it to learn meaningful patterns present in the data. Since the optimal number of fine-tuning epochs depends on the number of instances, the embedding dimension, and the LLM architecture, we implement an *early stopping criterion* to prevent overfitting.

Inference After fine-tuning, inference is performed by prompting the LLM with structured textual templates that mirror the training format, allowing it to autonomously generate new embedding rows.

Definition 2 (Textual inference) Given the embedding table $E \in \mathbb{R}^{I \times K}$, we define the set of inference prompts at each generation step as $\mathcal{P}^{\text{INF}} = \{\mathcal{P}_g^{\text{INF}}\}_{g=1}^G$ where:

$$\mathcal{P}_g^{\text{INF}} = \text{“Input: } \bigcirc_{k=1}^K (\text{value}_{\pi(k)} \text{ is [blank],) [sep] Target:”}$$

We use a multinomial distribution sampling strategy to reduce repetition and generate more creative and diverse outputs. The model draws from its learned token probability distribution at each step, guided by the temperature parameter, which controls sampling variability. As a result, all values are internally generated by the LLM in a fully conditional and self-contained manner, highlighting the model capacity to internalize statistical and structural patterns from compact embeddings and synthesize coherent time series without external noise injection or sampling routines.

At each inference step, we generate a batch of G synthetic instances, repeating the process until the desired number of sequences is obtained or a stopping criterion is met. We denote the set of all generated text instances as: $\mathcal{G} = \{\mathcal{G}_1, \dots, \mathcal{G}_G\}$. Ideally, the fine-tuned LLM should generate text instances in the following format: $\mathcal{G}_g = \bigcirc (\mathcal{P}_g^{\text{INF}}, \bigcirc_{k=1}^K (\tilde{a}_{g\pi(k)} \text{ [answer] }))$ where π is the random permutation used in $\mathcal{P}_g^{\text{INF}}$, and $\{\tilde{a}_{g\pi(k)}\}_{k=1}^K$ are the K numerical values inferred, which form the generated embedding table.

Retrieve embedding from text Given a generated text instance $\mathcal{G}_g \in \mathcal{G}$, we reconstruct the corresponding tabular data by mapping the inferred embedding values $\{\tilde{e}_{g\pi(k)}\}_{k=1}^K$ to their respective features. Each textual entry is split into feature-value pairs using “[answer]” as a delimiter. Missing or unrecognized features are assigned the placeholder “NaN”. For a specific channel c , the output of an inference step s is the reconstructed embedding matrix: $\tilde{E}^{c,s} \in \mathbb{R}^{G \times k_c}$, where each row corresponds to a generated instance \mathcal{G}_g and each column represents an inferred embedding feature associated with channel c . To track all generated embeddings up to step s , we define: $\tilde{E}^{c,\leq s}$.

In-generation filtering and stopping criterion At each inference step s , we apply an online filtering procedure that validates generated embeddings without requiring reconstruction into the time-series domain, ensuring efficient real-time evaluation. Specifically, the reconstructed embedding matrices $(\tilde{E}^{1,s}, \dots, \tilde{E}^{C,s})$ are filtered based on three criteria: 1) Instances with missing values are discarded, as they prevent accurate reconstruction; 2) Duplicated instances are discarded to maintain diversity in the generated dataset; 3) Significantly diverging instances are discarded. This combined filtering procedure not only enforces diversity and validity among the generated instances but also provides a diagnostic signal: if a substantial fraction of samples is rejected, it may indicate that the fine-tuned LLM requires further training or more representative data. Representative examples of

discarded instances and details on the divergence detection procedure are provided in Appendix A.3, while Appendix Table D.2 reports the rejection rates observed in a representative generation scenario, illustrating the balance between filtering rigor and sample diversity.

In generation mode, SDForger employs a dynamic stopping criterion that continues generating batches of G text instances as long as sufficient diversity is preserved among the generated samples (Appendix A.4). However, for consistent comparison with baseline methods across all simulation scenarios, we fix the number of generated instances \tilde{I} across all algorithms. If we denote by S the final inference step, then the output of the generation process is the complete embedding table $\tilde{E} \in \mathbb{R}^{\tilde{I} \times K}$, where, for each channel c , $\tilde{E}^c = \tilde{E}^{c, \leq S}$.

3.3 Decoding: from tabular embeddings to time series

Given \tilde{E} , the time-series representation of generated embeddings can be efficiently recovered due to the reversible nature of the embedding technique used. For the channel c , given the generated coefficients \tilde{e}_{ij}^c and the corresponding basis system $(b_1^c, \dots, b_{k_c}^c)$, the reconstructed time series are computed as follows Kokoszka and Reimherr (2017): $\tilde{x}_i^c = \sum_{j=1}^{k_c} \tilde{e}_{ij}^c b_j^c$.

This formulation ensures that each generated embedding is decoded back to the original space, resulting in \tilde{I} synthetic instances of a multivariate time series $\tilde{X}_i \in \mathbb{R}^{C \times L}$.

4 Evaluation methodology

Evaluation metrics Evaluating synthetic time-series data requires balancing *realism*, *usability*, and *efficiency*. A strong generative model should replicate key properties of real data while supporting downstream tasks such as forecasting. We adopt a comprehensive evaluation framework comprising two categories: *similarity metrics* and *utility metrics*.

- **Similarity metrics**, inspired by Ang et al. (2023), assess how closely the generated data matches the real data in terms of distribution, structure, and behavior. They fall into two subtypes: (i) **Feature-based metrics** which include *Marginal Distribution Difference (MDD)*, *Auto-Correlation Difference (ACD)*, *Skewness Difference (SD)*, and *Kurtosis Difference (KD)*, assess how well synthetic data retains key statistical properties of real data; (ii) **Distance-based metrics** include *Euclidean Distance (ED)*, *Dynamic Time Warping (DTW)*, and *SHAP-RE (SHR)*, a shapelet-based reconstruction error. They quantify the similarity between synthetic and real data in raw feature space or temporal alignment. Formal definitions are provided in Appendix B.
- Utility metrics assess the effectiveness of synthetic data in downstream tasks. Specifically, we fine-tune Tiny Time Mixers (TTM) (Ekambaram et al., 2024), a recent foundation model for multivariate time series, under four settings: (1) zero-shot (no fine-tuning) (2) real data only, (3) synthetic data only, and (4) real data augmented with synthetic data. This setup quantifies the impact of synthetic data on model transferability, data efficiency, and robustness.

Evaluation protocols We consider three distinct evaluation settings to assess the generative capabilities of SDForger across different structural assumptions:

- **Multisample generation** aims to produce new instances by combining patterns from multiple existing time series. This setting reflects scenarios such as generating experimental samples, weather profiles, or patient trajectories from heterogeneous observations. It emphasizes diversity and generalization in data-rich contexts.
- **Univariate generation** focuses on learning from a single time series to generate plausible alternative versions. This is useful for simulating counterfactual histories, seasonal variations, or stress-test scenarios in domains like finance, weather, and demand forecasting.
- **Multivariate generation** evaluates the ability to jointly generate multiple interdependent channels. It reflects real-world settings, such as energy systems, traffic flows, or sensor networks, where channel interactions and cross-correlations are crucial for realism and downstream utility.

In the multisample case, multiple instances are available by design. In contrast, for univariate and multivariate settings, only one instance is provided; therefore, we first apply the period-aware segmentation procedure described in Section 3 to extract multiple windows from each channel.

Parameter settings We summarize here the hyperparameters for SDForger. We fix the embedding dimension to $k = 3$ for the *multisample* and *univariate setting*. The LLM used for generation is GPT-2¹, fine-tuned with Adam (Diederik, 2014) optimization, a learning rate of 8×10^{-5} , batch size 32, and a maximum of 200 epochs. Early stopping criteria is applied based on the best validation loss computed every 5 steps, patience set to 5, randomly choosing 20% of the data as a validation set.

Baselines We evaluated SDForger’s performance against several baseline models for synthetic time series generation, covering different approaches. *Variational autoencoders*: TimeVAE (Desai et al., 2021), which models temporal dependencies with a recurrent VAE architecture, and TimeVQVAE (Lee et al., 2023), which incorporates vector quantization for better capturing discrete temporal patterns; *generative adversarial networks*: RTSGAN (Pei et al., 2021), which uses recurrent components for adversarial training, and SDEGAN (Kidger et al., 2021), which models time series as solutions to stochastic differential equations; and a *diffusion-based model*: LS4 (Zhou et al., 2023), which generates sequences via a learned reverse-time diffusion process. Hyperparameters for all baseline competitors follow those reported in their original papers, except for SdeGAN, for which we fix the number of training iterations to 1000 to balance convergence and computational cost.

Datasets We evaluated SDForger models using 12 publicly available datasets from various domains, including energy, transport, industry, weather, and finance, with sampling frequencies ranging from 2 minutes to monthly. The datasets, sourced from the Monash Time Series Forecasting Repository and other public domains, include both stationary and non-stationary time series, reflecting diverse temporal dynamics. Detailed information is provided in Appendix C.

5 Results

Following, we discuss results on **Similarity-based** (Section 5.1), **Utility-based metrics** (Section 5.2), and a condensed ablation study (Section 5.3). Complete ablations are provided in Appendix D.

5.1 Similarity-based metrics results

The similarity-based results aggregated for the multisample and univariate settings are reported in Table 1, with detailed per-dataset scores provided in Appendix Tables D.10, D.11, D.12, D.13, and D.14.

Overall performance. Different generative models exhibit complementary strengths: for instance, TimeVAE performs well on distribution-based metrics, while TimeVQVAE excels on distance-based measures such as Euclidean Distance and DTW. In contrast, *SDForger achieves consistently strong and balanced performance across both metric categories*, maintaining high scores without overfitting to either statistical or structural similarity (Table 1). This balanced behaviour is further confirmed by the normalized average scores per metric group and the average rank values. Such consistency indicates that SDForger not only preserves key statistical features but also captures the underlying temporal and distributional structure of the data, demonstrating strong generalization and robustness across heterogeneous temporal domains. By decoupling representation learning from generation, SDForger captures long-range dependencies while maintaining statistical realism, ultimately producing temporally coherent and domain-consistent synthetic samples.

Robustness to evaluation protocols Comparing multisample and univariate settings, we observe that model rankings and relative performances remain largely consistent, suggesting that SDForger is robust to variations in the evaluation protocol. This stability is an important advantage in practice, where test-time conditions may vary.

ICA vs. FPC The ICA embedding strategy consistently leads, particularly on distance-based metrics. The superior performance of the ICA-based variant likely comes from the nature of the components it produces. Unlike FPC, which orders components by explained variance and often concentrates most information in the first few components, ICA explicitly seeks statistically independent components. This tends to produce a more balanced and disentangled basis decomposition, where each component carries distinct information that have similar importance for data reconstruction. For our LLM-based generation pipeline, this disentanglement appears advantageous because the model can learn a joint

¹<https://huggingface.co/openai-community/gpt2>

Table 1: Aggregated performance comparison in the multisample and univariate settings. Metrics include raw similarity scores and normalized averages (in $[0 - 1]$) for each metric group, plus the average rank. Lower values are better. **Bold** indicates the best performance per column, and underlined indicates the second-best.

	Feature-based				Distance-based			Norm. Avg.			
	MDD	ACD	SD	KD	ED	DTW	SHR	Feat.	Dist.	Rank	
MULTISAMPLE	SDF-ICA ₃	0.244	<u>1.180</u>	0.869	2.384	16.669	12.373	6.870	<u>0.224</u>	0.074	3.143
	SDF-FPC ₃	0.255	2.166	1.323	4.299	17.749	11.921	16.537	0.562	0.100	4.714
	TimeVAE	0.227	0.259	0.507	1.697	18.041	<u>11.625</u>	14.021	0.000	0.094	2.143
	TimeVQVAE	0.371	5.466	1.327	3.889	13.661	10.167	2.030	0.873	0.000	3.714
	RtsGAN	0.279	1.769	<u>0.612</u>	<u>2.300</u>	<u>16.084</u>	11.859	<u>5.631</u>	0.231	<u>0.058</u>	<u>2.857</u>
	SdeGAN	<u>0.240</u>	2.098	1.404	4.091	37.174	33.391	51.678	0.540	0.693	5.286
LS4	0.276	6.150	1.243	4.852	44.389	31.806	160.403	0.789	0.977	6.143	
UNIVARIATE	SDF-ICA ₃	0.306	1.396	<u>0.671</u>	1.382	<u>18.802</u>	12.435	<u>4.856</u>	<u>0.149</u>	<u>0.070</u>	2.429
	SDF-FPC ₃	0.308	<u>1.480</u>	0.801	1.690	19.340	12.809	5.452	0.354	0.084	4.000
	TimeVAE	<u>0.288</u>	2.013	0.611	1.245	20.778	<u>12.126</u>	18.534	0.066	0.158	<u>2.714</u>
	TimeVQVAE	0.433	4.330	0.740	2.052	15.438	11.250	2.217	0.707	0.000	3.571
	RtsGAN	0.363	2.389	0.776	<u>1.325</u>	18.951	12.926	5.464	0.384	0.081	4.000
	SdeGAN	0.267	3.659	0.813	1.542	42.017	38.541	65.557	0.390	0.979	5.143
LS4	0.298	6.041	0.855	2.457	40.362	24.262	69.751	0.797	0.805	6.143	

Table 2: Utility evaluation via fine-tuned forecasting models. TTM forecasting performance on downstream tasks using different training sources: zero-shot, original data, generated data, and a combination of original and generated data. Results are reported for 3 multivariate datasets: *bikesharing* (target: count, control: temperature, humidity), *eth1* (target: HUFL, control: MUFL, OT), and *traffic* (target: junction1, control: junction2, junction3). Metrics include RMSE, MASE, WQL, and average rank (lower is better). **Bold** highlights the best result within each row group; underlined the second best; **bold+underlined** the overall best.

	bikesharing			eth1			traffic			Avg. Rank	
	RMSE	MASE	WQL	RMSE	MASE	WQL	RMSE	MASE	WQL		
0-shot	0.728	2.150	0.287	0.678	2.132	0.255	0.708	1.555	0.255	1.78	
Original Data (OD)	0.495	0.822	0.178	0.658	1.820	0.232	0.702	1.995	0.283	1.22	
GENERATED	SDF-ICA	0.514	<u>0.899</u>	0.194	0.626	1.820	0.224	0.655	1.849	<u>0.262</u>	2.00
	SDF-FPC	0.527	0.926	0.200	0.650	1.887	0.232	0.662	1.837	0.262	3.22
	TimeVAE	0.566	0.983	0.211	0.690	2.268	0.269	0.738	2.078	0.296	5.33
	TimeVQVAE	<u>0.520</u>	0.867	0.188	0.626	<u>1.874</u>	<u>0.227</u>	0.702	1.995	0.283	<u>2.67</u>
	RtsGAN	0.710	1.261	0.275	0.770	2.271	0.291	0.597	1.574	0.225	4.67
	SdeGAN	0.572	0.995	0.214	0.688	2.262	0.263	<u>0.629</u>	<u>1.715</u>	<u>0.243</u>	4.00
LS4	0.839	1.468	0.318	<u>0.642</u>	1.977	0.236	0.917	2.595	0.369	5.89	
ORIGINAL + GEN	SDF-ICA + OD	0.487	0.801	0.173	0.642	1.746	<u>0.226</u>	0.750	2.110	0.301	<u>3.22</u>
	SDF-FPC + OD	0.493	0.829	0.179	0.666	1.754	0.231	0.743	2.087	0.297	4.78
	TimeVAE + OD	<u>0.492</u>	0.814	0.176	0.654	<u>1.752</u>	0.228	0.721	2.039	0.290	2.89
	TimeVQVAE + OD	0.495	<u>0.804</u>	0.174	0.678	1.887	0.242	0.724	2.043	0.291	4.56
	RtsGAN + OD	0.498	0.819	0.177	<u>0.637</u>	1.872	0.231	<u>0.607</u>	1.647	0.234	3.44
	SdeGAN + OD	0.495	0.837	0.181	0.620	1.843	0.224	0.605	<u>1.716</u>	<u>0.242</u>	3.33
LS4 + OD	0.497	0.822	0.178	0.660	1.819	0.233	0.745	2.111	0.300	5.56	

distribution over a set of factors that all have the same “power”. Thus, the results suggest that the LLM is indeed better equipped to model the joint distribution when presented with independent factors rather than a hierarchy of variance-ordered components.

5.2 Utility-based metrics results

Table 2 presents the utility evaluation, where we assess the practical value of synthetic data by fine-tuning TTM on different multivariate training sources. For LS4, we modified the architecture to support multivariate generation. Furthermore, we adjust the embedding dimension k in SDForger according to the complexity of each dataset, setting $k=3$ for *bikesharing*, $k=7$ for *eth1*, and $k=5$

for *traffic*. To determine these values, we conducted a small ablation study to identify the optimal embedding dimension for each dataset (see Table D.7).

SDForger demonstrates strong performance across datasets, as evidenced by its top average rank, with notable results on *bikesharing* and *ethtl*. In *bikesharing*, synthetic data from SDForger alone yields competitive scores, and combining it with real data leads to the best overall performance across metrics. On *ethtl*, SDForger-generated data surpasses original data in RMSE and WQL, suggesting it captures critical temporal and statistical structure. The hybrid setting (original + generated) maintains this advantage and further improves MASE. Performance on *traffic* is more nuanced. Here, fine-tuning on real data is less effective, and GAN-based methods outperform others. Nevertheless, SDForger remains competitive, especially when using synthetic data alone. This suggests that the test distribution may deviate significantly from the training set, making traditional fine-tuning less useful. Indeed, high-quality synthetic data can act as a valuable supplement or even an alternative.

In no scenario does synthetic data degrade downstream performance, underscoring the reliability and utility of SDForger-generated samples across varied forecasting contexts.

5.3 Ablation

Effect of embedding dimension k Appendix Table D.6 presents an ablation study on the number of components k used in SDForger’s embedding space. A compact embedding with $k=3$ offers strong performance across both *multisample* and *univariate* settings, indicating that a small number of components is often sufficient to capture core temporal and structural patterns. However, the optimal value of k may vary across datasets, with more intricate dynamics potentially requiring higher-dimensional representations. In practice, users may also opt to select k based on a desired percentage of explained variance, adapting the representation to specific application needs.

Domain-level insights Appendix Tables D.3 and D.4 summarize the average normalized similarity scores per dataset. SDForger models achieve strong performance across a wide range of domains. Structured datasets such as *Energy*, *Appliances*, and *Weather* exhibit particularly high scores. In contrast, domains such as *Tourism*, *Traffic*, and *Finance* present greater challenges, likely due to their increased irregularity and noise. Nonetheless, SDForger maintains competitive results even in more complex settings, underscoring the flexibility of the proposed architecture.

Generation efficiency Appendix Table D.5 reports the average time to generate univariate sequences for three targets from the *Bikesharing* dataset, across two window lengths. SDForger is substantially faster than all competitors, often by one to two orders of magnitude. TimeVAE is the closest competitor but remains over $4\times$ slower. Notably, unlike GAN-based competitors, SDForger’s generation time is independent of sequence length and scales with the number of embedding components (k). A minor exception occurs at $k = 3$, where the reduced latent expressivity increases LLM fine-tuning time. Overall, SDForger achieves state-of-the-art efficiency without compromising quality.

LLM comparison GPT-2 (124M) achieves performance on par with, and sometimes better than larger and more recent models such as *granite-3.0* (2B) and *phi-3.5* (3.8B) (Appendix Table D.9). This shows that SDForger’s pipeline is effective even leveraging lightweight models. While runtime cost grows with model size, SDForger remains efficient compared to baselines (Appendix Table D.8).

Filtering Procedure. Appendix Table D.2 reports rejection statistics for a representative generation scenario. We observe that the overall discard rate remains consistently low ($< 2\%$) across settings, indicating that most generated embeddings fall within a plausible norm range. The proportion of missing values increases with larger embedding dimensions, reflecting a higher likelihood of incomplete generations in longer textual outputs. Notably, the ℓ_2 norms of accepted samples closely match those of the original embeddings, while discarded ones exhibit markedly higher values, confirming that the filtering procedure effectively removes divergent or anomalous generations.

6 Shaping time series with language

SDForger is designed to naturally incorporate textual information, making it well-suited for state-of-the-art time-series generation that embraces additional multi-modal inputs. To explore this, we conduct an experiment using the *bikesharing* dataset. Coming from the intuition that these variables stem from a common physical process and may share latent components, we embed their three

channels (temperature, count, and humidity) into a shared ICA basis. We incorporate the channel information in the textual encoder: “Condition: data is temp [sep] Input: value_1 is [blank]... [sep] Target: e_{i1} [answer]...”

This conditioning strategy enables SDForger to generate channel-specific sequences with high fidelity. For instance, using a longitudinal k -nearest neighbor classifier (Ramos-Carreño et al., 2024) trained on real data, we achieve an accuracy of 0.81 in identifying the generated curves (see Figure 2). These results highlight SDForger’s strong generative capacity and its ability to integrate and respond to textual cues, positioning it as a flexible and powerful baseline for multimodal time-series synthesis.

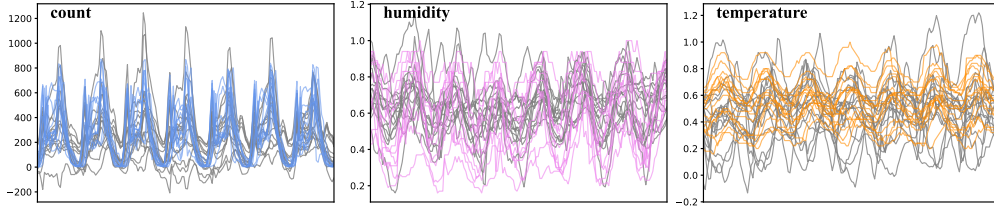


Figure 2: Text-Conditioned Generation with SDForger. Visualization of 10 original (grey) and synthetic samples per channel from the *bikesharing* data. Synthetic data is generated using conditional prompts: “Condition: data is cnt (blue)”, “Condition: data is hum (pink)”, and “Condition: data is temp (orange)”.

7 Conclusions

We introduced **SDForger**, a flexible and efficient framework for generating synthetic multivariate time series using large language models. By combining compact functional embeddings with textual conditioning, SDForger enables high-quality generation even in data-scarce settings. Extensive evaluations across multiple datasets and tasks demonstrate that SDForger consistently achieves strong similarity scores and enhances downstream forecasting performance—often matching or surpassing results obtained from real data and outperforming state-of-the-art baselines.

Ablation studies confirm the robustness of the framework across embedding strategies, dimensionality choices, and LLM architectures. SDForger is also highly efficient, with significantly lower generation times compared to its competitors. Moreover, by leveraging LLMs, SDForger enables seamless integration with textual prompts, paving the way for multimodal time-series generation, where natural language can guide not only content but also structure, semantics, or temporal context.

We believe SDForger can be further improved. Its modular design is intentionally built to support flexible experimentation, making it easy to explore enhancements or tailor components to specific needs. We see several promising directions:

- **Embedding Strategies** While our current approach relies on linear methods like FastICA and FPC, future work could explore more expressive, nonlinear embeddings (e.g., AE) or multivariate-aware methods like Multivariate FPCA or Multivariate Singular Spectrum Analysis to better capture temporal and inter-channel dependencies.
- **Parameter-Efficient Fine-Tuning** We currently use full fine-tuning for the LLM. However, using too many components relative to the number of instances can lead to unstable fine-tuning and reduced generation quality. Incorporating PEFT techniques such as LoRA or adapters could improve scalability, efficiency, and facilitate domain adaptation.
- **Extension to encoder-only models** Our current implementation supports only autoregressive LLMs; future work would extend the framework to encoder-only models and different generation paradigms such as masked token prediction.
- **Extended Utility Evaluation** While we focus on forecasting, SDForger could be evaluated and optimized for broader downstream tasks such as classification or anomaly detection.
- **Context and Covariate Integration** By design, SDForger supports integration of external covariates (e.g., categorical or textual data). Expanding this functionality could enable richer conditional generation, and multimodal transfer learning (see Section 6).

In summary, SDForger offers a flexible foundation, and we see meaningful opportunities to improve it both architecturally and in terms of task generalization.

References

- Ang, Y., Q. Huang, Y. Bao, A. K. Tung, and Z. Huang (2023). Tsgbench: Time series generation benchmark. *Proc. VLDB Endow.* 17(3), 305–318.
- Ansari, A. F., L. Stella, C. Turkmen, X. Zhang, P. Mercado, H. Shen, O. Shchur, S. S. Rangapuram, S. P. Arango, S. Kapoor, et al. (2024). Chronos: Learning the language of time series. *arXiv preprint arXiv:2403.07815*.
- Borisov, V., K. Seßler, T. Leemann, M. Pawelczyk, and G. Kasneci (2022). Language models are realistic tabular data generators. *arXiv preprint arXiv:2210.06280*.
- Boschi, T., L. Testa, F. Chiaromonte, and M. Reimherr (2024). Fasten: an efficient adaptive method for feature selection and estimation in high-dimensional functional regressions. *Journal of Computational and Graphical Statistics*, 1–13.
- Desai, A., C. Freeman, Z. Wang, and I. Beaver (2021). Timevae: A variational auto-encoder for multivariate time series generation. *arXiv preprint arXiv:2111.08095*.
- Diederik, K. (2014). Adam: A method for stochastic optimization. (*No Title*).
- Donahue, C., M. Lee, and P. Liang (2020). Enabling language models to fill in the blanks. *arXiv preprint arXiv:2005.05339*.
- Ekambaram, V., A. Jati, N. H. Nguyen, P. Dayama, C. Reddy, W. M. Gifford, and J. Kalagnanam (2024). Ttms: Fast multi-level tiny time mixers for improved zero-shot and few-shot forecasting of multivariate time series. *arXiv preprint arXiv:2401.03955*.
- Garza, A. and M. Mergenthaler-Canseco (2023). Timegpt-1. *arXiv preprint arXiv:2310.03589*.
- Godahewa, R., C. Bergmeir, G. I. Webb, R. J. Hyndman, and P. Montero-Manso (2021). Monash time series forecasting archive. *arXiv preprint arXiv:2105.06643*.
- Gruver, N., M. Finzi, S. Qiu, and A. G. Wilson (2024). Large language models are zero-shot time series forecasters. *Advances in Neural Information Processing Systems* 36.
- Hyvarinen, A. (1999). Fast ica for noisy data using gaussian moments. In *1999 IEEE international symposium on circuits and systems (ISCAS)*, Volume 5, pp. 57–61. IEEE.
- Jablonka, K. M., C. Charalambous, E. Sanchez Fernandez, G. Wiechers, J. Monteiro, P. Moser, B. Smit, and S. Garcia (2023). Machine learning for industrial processes: Forecasting amine emissions from a carbon capture plant. *Science Advances* 9(1), eadc9576.
- Jin, M., S. Wang, L. Ma, Z. Chu, J. Y. Zhang, X. Shi, P.-Y. Chen, Y. Liang, Y.-F. Li, S. Pan, et al. (2023). Time-llm: Time series forecasting by reprogramming large language models. *arXiv preprint arXiv:2310.01728*.
- Kidger, P., J. Foster, X. Li, and T. J. Lyons (2021). Neural sdes as infinite-dimensional gans. In *International conference on machine learning*, pp. 5453–5463. PMLR.
- Kit, A., A. Järvinen, Y. Poels, S. Wiesen, V. Menkovski, R. Fischer, M. Dunne, A.-U. Team, et al. (2024). On learning latent dynamics of the aug plasma state. *Physics of Plasmas* 31(3).
- Kokoszka, P. and M. Reimherr (2017). *Introduction to functional data analysis*. CRC Press.
- Lee, D., S. Malacarne, and E. Aune (2023). Vector quantized time series generation with a bidirectional prior model. *arXiv preprint arXiv:2303.04743*.
- Liang, Y., H. Wen, Y. Nie, Y. Jiang, M. Jin, D. Song, S. Pan, and Q. Wen (2024). Foundation models for time series analysis: A tutorial and survey. In *Proceedings of the 30th ACM SIGKDD conference on knowledge discovery and data mining*, pp. 6555–6565.
- Lim, B., S. Ö. Arik, N. Loeff, and T. Pfister (2021). Temporal fusion transformers for interpretable multi-horizon time series forecasting. *International Journal of Forecasting* 37(4), 1748–1764.

- Padhi, I., Y. Schiff, I. Melnyk, M. Rigotti, Y. Mroueh, P. Dognin, J. Ross, R. Nair, and E. Altman (2021). Tabular transformers for modeling multivariate time series. In *ICASSP 2021-2021 IEEE International Conference on Acoustics, Speech and Signal Processing (ICASSP)*, pp. 3565–3569. IEEE.
- Pei, H., K. Ren, Y. Yang, C. Liu, T. Qin, and D. Li (2021). Towards generating real-world time series data. In *2021 IEEE International Conference on Data Mining (ICDM)*, pp. 469–478. IEEE.
- Ramos-Carreño, C., J. L. Torrecilla, M. Carbajo-Berrocal, P. Marcos, and A. Suárez (2024). scikit-fda: a python package for functional data analysis. *Journal of Statistical Software* 109, 1–37.
- Ramsay, J. O. and B. W. Silverman (2005). *Functional data analysis* (2 ed.). Springer.
- Seyfi, A., J.-F. Rajotte, and R. Ng (2022). Generating multivariate time series with common source coordinated gan (cosci-gan). *Advances in neural information processing systems* 35, 32777–32788.
- Smith, K. E. and A. O. Smith (2020). Conditional gan for timeseries generation. *arXiv preprint arXiv:2006.16477*.
- Zheng, G., Y. Yang, and J. Carbonell (2016). Efficient shift-invariant dictionary learning. In *Proceedings of the 22nd ACM SIGKDD International Conference on Knowledge Discovery and Data Mining*, pp. 2095–2104.
- Zhou, L., M. Poli, W. Xu, S. Massaroli, and S. Ermon (2023). Deep latent state space models for time-series generation. In *International Conference on Machine Learning*, pp. 42625–42643. PMLR.
- Zhou, T., P. Niu, L. Sun, R. Jin, et al. (2023). One fits all: Power general time series analysis by pretrained lm. *Advances in neural information processing systems* 36, 43322–43355.
- Zhou, Y., L. You, W. Zhu, and P. Xu (2023). Improving time series forecasting with mixup data augmentation.

Appendix

A Implementation details

A.1 Data preprocessing: segmentation

In many scenarios, each channel consists of a single historical time series, i.e., $I_0 = 1$. However, to estimate embeddings that effectively capture the temporal distribution, multiple instances per channel are necessary. Therefore, when $I_0 = 1$, we segment each channel into multiple overlapping windows. Specifically, for each channel c , we construct I_c windows of fixed length L_c , where $L_c < L_0$. Without loss of generality, for simplicity in notation, we assume L_c and I_c are identical across all channels and denote them as L and I , respectively.

To ensure robust learning of the embedding distribution, I must be sufficiently large. Our experiments indicate that even $I = 15$ (i.e., 15 instances) suffices for this purpose. Once I and L are fixed, we segment the time series while minimizing the overlap between consecutive windows. The overlap step is determined by the dominant periodicity P of the channel, ensuring that window transitions align with intrinsic temporal cycles.

The set of extracted windows \mathcal{W} is formally defined as:

$$\mathcal{W} = \{X[t : t + L] \mid t = 0, s, 2s, \dots, L_0 - L\} \quad (1)$$

where the step size s is computed as: $s = \max(1, \lfloor \frac{L_0 - L}{I - 1} \rfloor)$ and then adjusted to be the nearest multiple of P to maintain consistency in periodic structure.

To determine the dominant periodicity P , we employ the Autocorrelation Function (ACF), which quantifies the similarity between the time series and its lagged versions at different time shifts. This method is robust to noise and remains effective even when periodicity is not strictly stationary.

The estimation of P follows these steps:

1. Compute the ACF and identify significant peaks, excluding lag 0.
2. Rank the detected peaks by their autocorrelation values.
3. Select the highest-ranked period P such that $P < L/2$.

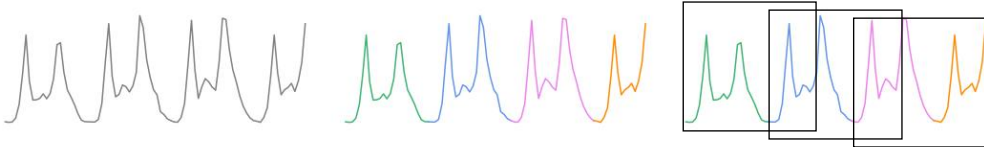


Figure A.1: Periodicity-aware segmentation.

By leveraging this periodicity-aware segmentation strategy, we ensure that the extracted windows align with the natural cycles of the time series. Moreover, this approach minimizes window overlap, maximizing their independence and diversity and facilitating more effective embedding computations for downstream generative tasks.

This pre-processing transforms the data from a single sequence X_1 into a set $X = \{X_i\}_{i=1}^I$, where each $X_i \in \mathbb{R}^{C \times L}$, preparing the data for the generation task.

A.2 Choice of the number of components

The choice of k_c determines how well the basis representation approximates the original time-series channel c . Our framework allows the user to either select the smallest k_c that explains a predefined percentage of the total variance of the original time series or manually specify k_c .

There exists an inherent trade-off in selecting k_c . A higher k_c captures more of the total variability but can hinder the LLM’s ability to model the underlying distribution during the generation phase. Moreover, if k_c is too large, the generated samples may become overly similar to the original data,

limiting diversity and the introduction of novel patterns. Conversely, choosing k_c too small risks omitting essential structures and temporal characteristics, degrading the reconstruction quality.

It is important to note that the nature of the components differs between FPC and FastICA. FPC forms a parsimonious basis system, where a few components typically suffice to capture most of the variability, with components ordered by the amount of variance they explain—early components being systematically more informative. In contrast, FastICA components are unordered: each component contributes independently, without a hierarchical importance structure. As a result, FastICA generally requires more components to achieve a similar reconstruction quality compared to FPC. However, this property also makes FastICA embeddings more robust during generation, as information is distributed more evenly across components, reducing the risk that a few badly generated components disproportionately affect the synthesized curves.

To provide a quantitative intuition, Appendix Table D.1 reports the proportion of variance retained across embedding dimensions for both decomposition methods. This analysis highlights how the variance explained increases with k , and how FPC typically achieves higher cumulative variance with fewer components, while FastICA distributes information more evenly across dimensions.

In practice, we recommend keeping the total number of components K reasonably small, particularly when the number of training instances is limited. Empirically, with a training set of 30 instances, setting $K > 25$ often results in unstable fine-tuning and an increased rate of discarded samples due to low-quality generation. This limitation stems from the LLM’s reduced ability to model high-dimensional embeddings under data-scarce conditions effectively.

A.3 In-generation filtering

Missing values and duplicated instances. To illustrate the filtering logic, we report three concrete examples of generated prompts with embedding dimension $K = 4$. Following the inference template:

$$\mathcal{P}_g^{\text{INF}} = \text{“Input: } \bigcirc_{k=1}^K (\text{value_}\pi(k) \text{ is [blank],) [sep] Target:”},$$

the model produces the following textual generations:

- **Prompt 1 (valid)**
 Input: value_2 is [blank], value_4 is [blank], value_1 is [blank], value_3 is [blank] [sep] Target: 0.125 [answer] -0.084 [answer] 0.217 [answer] 0.041 [answer]
- **Prompt 2 (duplicated)**
 Input: value_4 is [blank], value_1 is [blank], value_2 is [blank], value_3 is [blank] [sep] Target: -0.084 [answer] 0.217 [answer] 0.125 [answer] 0.041 [answer]
- **Prompt 3 (missing value)**
 Input: value_1 is [blank], value_3 is [blank], value_2 is [blank], value_4 is [blank] [sep] Target: 0.182 [answer] 0.095 [answer] -0.012 [answer]

In this example, the filtering stage identifies *Prompt 2* as a duplicate of *Prompt 1* and discards it, while *Prompt 3* is removed because it does not contain all the targets’ coefficients. Only *Prompt 1* is retained for reconstruction. This simple yet effective procedure ensures that the generated embedding tables remain diverse and valid before decoding into the time-series domain.

Diverging instances To ensure the quality of synthetic data, we discard generated instances whose embedding coefficients significantly deviate from the distribution of the original data. Specifically, we compute the squared ℓ_2 -norm of each embedding vector and compare it to the norms of the original embeddings. This criterion efficiently filters out extreme outliers in the latent space, without requiring reconstruction into the time-series domain.

Formally, for each channel c , let $\hat{E}^{c,s} = E^c \cup \tilde{E}^{c,\leq s-1}$ be the matrix containing both original embeddings and all previously accepted generated embeddings up to inference step $s - 1$, with $\hat{E}^{c,0} = E^c$. Denote by $N^{c,\text{old}}$ and $N^{c,\text{new}}$ the sets of squared Euclidean norms of the rows of $\hat{E}^{c,s-1}$

and the newly generated matrix $\tilde{E}^{c,s}$, respectively. For each newly generated row i , we compute its norm and accept it only if:

$$q_1 - 3 \cdot \text{IQR} \leq N_i^{c,\text{new}} \leq q_3 + 3 \cdot \text{IQR},$$

where q_1 and q_3 are the first and third quartiles of $N^{c,\text{old}}$, and $\text{IQR} = q_3 - q_1$. An instance is retained only if this condition is satisfied across all channels c .

This norm-based strategy is particularly well-motivated when using FPCs, due to the orthonormality of the basis. Let \mathcal{X}_i^c be a time series in channel c and b_j^c the corresponding FPC basis. Then the \mathbb{L}^2 -norm of \mathcal{X}_i^c can be approximated by the Euclidean norm of its FPC coefficients:

$$\int_{\mathcal{T}} (\mathcal{X}_i^c)^2 dt = \|\mathcal{X}_i^c\|_{\mathbb{L}^2}^2 = \sum_{j=1}^{\infty} \langle \mathcal{X}_i^c, b_j^c \rangle_{\mathbb{L}^2}^2 \approx \sum_{j=1}^{k_c} (e_{ij}^c)^2,$$

where e_{ij}^c are the FPC embedding coefficients. This justifies the norm-based filtering as a direct proxy for detecting time-series samples with unusually high or low energy.

While filtering based on coefficient norms does not guarantee full statistical fidelity to the original time-series distribution, it serves as an effective mechanism to remove extreme outliers without reconstruction. Combined with additional checks for missing values and duplicates, this step helps preserve both the *diversity* and *relevance* of the generated data. A high rejection rate may indicate insufficient LLM fine-tuning or poor generalization, suggesting the need for more representative training data or additional training steps.

A.4 Stopping criterion

The stopping criterion monitors the diversity of the generated norms across all channels to determine when the generation process should stop. When using FPC, these norms correspond to the \mathbb{L}^2 -norms of the generated curves. When using FastICA, they correspond to the norms of the embedding coefficient vectors; although not directly related to the curve norms, they still provide a useful proxy for identifying over-sampling and loss of variability.

At inference step s , for each channel c , let u^c denote the number of unique values in $N^{c,\text{old}}$ (the set of accepted norms up to step s), rounded to the fourth decimal place. Let \tilde{I} be the total number of valid instances generated so far. We define the *diversity score* for channel c as:

$$D^c = u^c / \tilde{I}.$$

The diversity score provides a quantitative measure of how much variability remains in the generated norms. We track D^c at each inference step, and the stopping condition is triggered when:

$$\max_c D^c < \lambda_{\text{stop}} \quad \text{or} \quad \tilde{I} > \tilde{I}_{\text{max}}.$$

In other words, generation stops either when the maximum diversity score across channels falls below a predefined threshold λ_{stop} , indicating reduced novelty, or when the total number of generated instances exceeds a maximum cap \tilde{I}_{max} .

Monitoring the diversity score enables us to assess whether the model continues to introduce new variability in the generated data, serving as an online signal for generation quality.

If we denote by S the final inference step, then the output of the generation process is the complete embedding table $\tilde{E} \in \mathbb{R}^{\tilde{I} \times K}$, where, for each channel c , $\tilde{E}^c = \tilde{E}^{c,\leq S}$.

B Evaluation metrics

All the metrics presented below are adopted from Ang et al. (2023), except for *Shapelet-based Reconstruction*, which follows the definition in Zheng et al. (2016).

B.1 Feature-based evaluation

Marginal Distribution Difference MDD computes an empirical histogram for each dimension and time step in the generated series, using the bin centers and widths from the original series. It then calculates the average absolute difference between this histogram and that of the original series across bins, assessing how closely the distributions of the original and generated series align.

AutoCorrelation Difference ACD computes the autocorrelation of both the original and generated time series, then determines their difference. By contrasting the autocorrelations, we could evaluate how well dependencies are maintained in the generated time series.

Skewness Difference SD is vital for the marginal distribution of a time series, quantifying its distribution asymmetry. Given the mean (standard deviation) of the train time series T_s^{tr} as μ_s^{tr} (σ_s^{tr}) and the generated time series T_s^{gen} as μ_s^{gen} (σ_s^{gen}), we evaluate the fidelity of T_s^{gen} by computing the skewness difference between them as:

$$SD = \left| \frac{\mathbb{E}[(T_s^{gen} - \mu_s^{gen})^3]}{\sigma_s^{gen3}} - \frac{\mathbb{E}[(T_s^{tr} - \mu_s^{tr})^3]}{\sigma_s^{tr3}} \right|.$$

Kurtosis Difference Like skewness, KD assesses the tail behavior of a distribution, revealing extreme deviations from the mean. Using the previous notations, the kurtosis difference between T_s^{tr} and T_s^{gen} is calculated as:

$$KD = \left| \frac{\mathbb{E}[(T_s^{gen} - \mu_s^{gen})^4]}{\sigma_s^{gen4}} - \frac{\mathbb{E}[(T_s^{tr} - \mu_s^{tr})^4]}{\sigma_s^{tr4}} \right|.$$

B.2 Distance-based evaluation

Euclidean Distance For each original series $s^{tr} = (x_1, \dots, x_l)$ and its generated $s^{gen} = (y_1, \dots, y_l)$, $ED = \sqrt{\sum_{i=1}^l (x_i - y_i)^2}$. We take the mean of ED for all series and all samples. Given that the input time series has been preprocessed to fit within the range of $[0, 1]$, ED deterministically assesses the similarity between s^{gen} and s^{tr} . It provides a value-wise comparison between the time series.

Dynamic Time Warping Given that ED overlooks alignment, we include DTW to capture the optimal alignment between series regardless of their pace or timing. The alignment facilitated by DTW offers insights into the predictive quality of the generated series.

Shapelet-based Reconstructions Shapelet based RE is calculated by generated time series using shapelets extracted using shift invariant dictionary learning (SIDL) algorithm (Zheng et al., 2016). Shapelets represent local discriminative patterns present in the time-series data. We learn shift invariant patterns/shapelets on the original time-series dataset and then use the learnt dictionary to reconstruct unseen generated time series. The reconstruction error is calculated between the generated time series and their reconstruction using SIDL.

C Datasets & protocol settings

Table C.1: Overview of the benchmark datasets. For each dataset, we report its application domain, sampling frequency, number of time series, length statistics, and the type of evaluation (univariate, multivariate, multi-sample) it supports.

Dataset	Domain	Freq.	Number	Evaluation type		
				MS	UV	MV
Australian Electricity	energy	30m	5	N	Y	Y
Appliances	energy	10m	1	N	Y	N
Bikesharing	general	1H	3	N	Y	Y
Carbon Capture Plant	nature	2m	4	N	Y	N
ETTH1	energy	1H	3	N	Y	Y
ECL	energy	1H	320	Y	N	N
Exchange Rate	finance	1D	8	N	Y	N
NN5	finance	1D	111	Y	N	N
Tourism	general	1M	365	Y	N	N
Traffic	transport	1H	3	N	Y	Y
Traffic Monash	transport	1H	861	Y	N	N
Solar - Weather	nature	1H	653	Y	N	N
Rain - Weather	nature	1H	386	Y	N	N
Temperature - Weather	nature	1H	362	Y	N	N

C.1 Dataset overview

Energy

- *Australian Electricity* (Godaheva et al., 2021) contains electricity demand data from 5 states in Australia.
- *Appliances*² contains house temperature and humidity conditions monitored with a wireless sensor network, and energy data logegd with m-bus energy meters averaged for 10 minutes periods.
- *ETTH1*³ contains oil temperatures and other covariates of electrical transformers from two stations in China, measured at 15 minutes granularity but hourly aggregated.
- *ECL*⁴ contains electricity consumption of 370 points.

Mobility and Transport

- *Bikesharing*⁵ contains the hourly and daily count of rental bikes between the years 2011 and 2012 in the Capital bike share system with the corresponding weather and seasonal information.
- *Traffic*⁶ contains observations of the number of vehicles each hour in four different junctions
- *Traffic Monash* (Godaheva et al., 2021) contains hourly road occupancy readings from sensors in the San Francisco Bay area.
- *Tourism* (Godaheva et al., 2021) dataset from, used for the Kaggle Tourism Forecasting competition. This dataset is non-stationary.

Nature

- *Carbon Capture Plant* (Jablonka et al., 2023) records the emission profiles of “2-amino-2-methyl-1-propanol” (AMP) and “piperazine” (Pz) collected at every 2 minutes interval.
- *Weather* (Godaheva et al., 2021) contains daily time series of four weather variables (rain, mintemp, maxtemp and solar radiation) measured at weather stations in Australia.

Finance

²<https://www.kaggle.com/datasets/loveall/appliances-energy-prediction>

³<https://github.com/zhouhaoyi/ETDataset>

⁴<https://www.kaggle.com/datasets/minhnguyendichnhat/ecl-dataset>

⁵<https://www.kaggle.com/datasets/lakshmi25npathi/bike-sharing-dataset>

⁶<https://www.kaggle.com/datasets/fedesoriano/traffic-prediction-dataset>

- *Exchange Rate* (Godaheva et al., 2021) contains daily exchange rates for currencies of eight countries (Australia, British, Canada, Switzerland, China, Japan, New Zealand and Singapore) between 1990 and 2016. This dataset is non-stationary.
- *NN5 (Daily, Weekly)* (Godaheva et al., 2021) contains cash withdrawal data from ATMs. This dataset combines stationary and non-stationary time series.

C.2 Protocols

Multisample setting For MS data preparation, we sampled $I = 30$ instances, each of length $L = 250$, resulting in a total training sequence of 15,000 timestamps. Standard scaling per timestamp is applied. For evaluation, we generate 100 synthetic instances.

Univariate setting For UV data preparation, we used a training sequence of length $L_0 = 2,000$, segmented into $I = 30$ instances of length $L = 250$ using our periodicity-aware segmentation strategy (cf Appendix A.1). Same standard scaling was applied. For evaluation, we generate 100 synthetic instances.

Multivariate setting For fine-tuning TTM in the MV setting, we used consecutive sequences of length $L_0 = 5000, 2500,$ and 2500 for training, validation, and testing, respectively. Each set was segmented into $I = 30, 15,$ and 15 instances of length $L = 1120$ using our period-aware segmentation strategy (Appendix A.1). Periodicity was estimated from the training set. Standard scaling per timestamp, computed on the training set, was applied consistently across all splits. For evaluation, we generated 30 instances, matching the size of the training set.

D Additional results

Table D.1: Variance retained across embedding dimensions. For each dataset, we report the proportion of total variance retained for embedding dimensions $k = 3, k = 5,$ and $k = 7$ under both FastICA and FPC decompositions.

Dataset	FICA			FPC		
	k=3	k=5	k=7	k=3	k=5	k=7
Appliances	0.333	0.457	0.539	0.324	0.459	0.555
Australian Electricity	0.703	0.853	0.912	0.787	0.895	0.938
Bikesharing	0.492	0.662	0.744	0.599	0.734	0.796
Carbon Capture Plant	0.773	0.905	0.951	0.843	0.933	0.965
ETTH1	0.536	0.686	0.775	0.635	0.754	0.823
ECL	0.809	0.941	0.971	0.991	0.997	0.999
Exchange Rate	0.776	0.907	0.942	0.957	0.982	0.989
NN5	0.336	0.479	0.590	0.719	0.780	0.826
Tourism	0.869	0.954	0.977	0.986	0.995	0.998
Traffic	0.376	0.564	0.697	0.408	0.591	0.714
Traffic Monash	0.541	0.722	0.823	0.745	0.845	0.902
Rain - Weather	0.449	0.605	0.725	0.558	0.684	0.781
Solar - Weather	0.450	0.616	0.718	0.674	0.773	0.833
Temperature Max - Weather	0.493	0.602	0.685	0.864	0.893	0.915
Temperature Min - Weather	0.390	0.517	0.611	0.777	0.824	0.858

Table D.2: Filtering statistics for generated embeddings. Rejection statistics on the *count* variable from the *bikesharing* dataset, averaged across 5 seeds. Each row reports the proportion of generated samples containing missing values, the fraction of samples discarded by the filtering stage, and the average ℓ_2 norms of the original, accepted, and discarded embedding vectors.

	NaN%	Discard%	Norms Original (Avg)	Norms Accepted (Avg)	Norms Discarded (Avg)
SDF-ICA ₃	3.87	1.94	1.708	1.714	19.066
SDF-ICA ₅	36.29	1.94	2.202	2.248	9.514
SDF-ICA ₇	58.82	0.00	2.602	2.521	0.000

Table D.3: Per-dataset similarity results in the multisample setting. Average normalized similarity scores (feature-based and distance-based) for each dataset and model.

	Feature-Based					Distance-Based				
	ecl	nn5	tourism	traffic	weather	ecl	nn5	tourism	traffic	weather
SDF-ICA ₃	0.402	<u>0.195</u>	0.268	0.330	<u>0.204</u>	<u>0.018</u>	0.129	<u>0.032</u>	0.086	0.137
SDF-FPC ₃	0.576	0.323	0.594	<u>0.293</u>	0.296	0.054	0.183	0.073	0.099	0.136
TimeVAE	<u>0.164</u>	0.109	<u>0.211</u>	0.143	0.174	0.063	0.139	0.074	0.143	0.125
TimeVQVAE	0.754	0.380	0.818	0.437	0.498	0.003	0.068	0.009	0.053	0.069
RtsGAN	0.049	0.347	0.174	0.344	0.315	0.075	<u>0.074</u>	0.110	<u>0.059</u>	<u>0.102</u>
SdeGAN	0.499	0.219	0.539	0.391	0.308	0.299	0.652	0.290	0.496	0.616
LS4	0.860	0.319	0.849	0.470	0.400	0.720	0.681	0.639	0.926	0.707

Table D.4: Per-dataset similarity results in the univariate setting. Average normalized similarity scores (feature-based and distance-based) for each dataset and model.

	Feature-Based							Distance-Based						
	appl.	austr.	bike	carbon	eth1	exch.	traffic	appl.	austr.	bike	carbon	eth1	exch.	traffic
SDF-ICA ₃	<u>0.486</u>	0.122	0.162	<u>0.197</u>	<u>0.128</u>	0.155	0.269	0.088	0.073	<u>0.077</u>	<u>0.063</u>	0.080	0.115	0.059
SDF-FPC ₃	0.509	0.122	<u>0.169</u>	0.345	0.107	0.287	0.213	0.085	0.101	<u>0.077</u>	0.078	0.076	0.143	0.064
TimeVAE	0.370	0.123	0.184	0.176	0.234	0.113	<u>0.236</u>	0.119	0.079	0.155	0.102	0.140	<u>0.091</u>	0.178
TimeVQVAE	0.531	0.439	0.371	0.572	0.354	0.578	0.312	0.045	0.031	0.037	0.005	0.031	0.031	0.035
RtsGAN	0.567	0.300	0.273	0.226	0.244	0.217	0.312	<u>0.056</u>	0.098	0.084	0.085	<u>0.072</u>	0.157	<u>0.053</u>
SdeGAN	0.634	0.128	0.174	0.409	0.173	<u>0.115</u>	0.249	0.456	0.623	0.831	0.703	0.833	0.469	0.765
LS4	0.609	0.294	0.265	0.695	0.289	0.416	0.300	0.720	0.471	0.475	0.554	0.364	0.498	0.621

Table D.5: Average generation time: baselines Average time (in seconds) required to generate synthetic univariate time series for the bikesharing dataset across three targets: count, temperature, and humidity. We report results for two input sequence lengths: 250 and 500. All models were evaluated under the same computational constraints (-mem 20G -cores 1+1 -gpu v100) using a single NVIDIA V100 GPU.

Length	SDF-ICA ₃	SDF-ICA ₅	SDF-ICA ₇	SDF-FPC ₃	SDF-FPC ₅	SDF-FPC ₇	TimeVAE	TimeVQVAE	RtsGAN	SdeGAN	LS4
250	41.9	26.8	28.8	22.0	25.4	33.1	138.1	4574.2	2055.7	3498.9	2804.4
500	38.3	22.8	26.0	17.9	22.8	26.6	112.6	4401.4	3536.3	7316.7	2378.9

Table D.6: Ablation study: embedding dimension. Aggregated similarity-based performance across all datasets in the multisample and univariate setting.

	Feature-based				Distance-based			Norm. Avg.		
	MDD	ACD	SD	KD	ED	DTW	SHR	Feat.	Dist.	
MULTISAMPLE	SDF-FPC ₃	<u>0.255</u>	2.166	<u>1.323</u>	4.299	17.749	11.921	16.537	0.616	0.609
	SDF-FPC ₅	0.262	3.191	1.336	3.668	17.475	<u>11.727</u>	22.893	0.714	0.535
	SDF-FPC ₇	0.264	3.534	1.500	3.560	17.710	11.652	28.068	0.787	0.655
	SDF-ICA ₃	0.244	1.180	0.869	2.384	16.669	12.373	6.870	0.050	<u>0.333</u>
	SDF-ICA ₅	0.261	<u>0.782</u>	1.378	<u>2.649</u>	<u>16.743</u>	12.238	<u>7.731</u>	<u>0.371</u>	0.307
	SDF-ICA ₇	0.265	0.589	1.964	2.963	16.900	12.031	14.195	0.576	0.362
UNIVARIATE	SDF-FPC ₃	0.308	1.480	0.801	1.690	19.340	12.809	<u>5.452</u>	0.736	0.469
	SDF-FPC ₅	0.306	1.887	0.773	1.581	20.534	12.513	8.920	0.536	0.753
	SDF-FPC ₇	0.309	2.399	0.774	1.954	20.470	12.079	10.982	0.947	0.654
	SDF-ICA ₃	<u>0.306</u>	1.396	0.671	<u>1.382</u>	18.802	12.435	4.856	0.169	0.163
	SDF-ICA ₅	0.306	<u>0.867</u>	0.770	1.333	<u>19.043</u>	<u>12.261</u>	6.555	0.279	<u>0.222</u>
	SDF-ICA ₇	0.306	0.597	<u>0.736</u>	1.458	19.989	12.381	8.102	<u>0.175</u>	0.543

Table D.7: Ablation study: embedding dimension. TTM forecasting performance on downstream tasks using different training sources: generated data, and a combination of original and generated data. Results are reported for 3 multivariate datasets: *bikesharing* (target: count, control: temperature, humidity), *eth1* (target: HUFL, control: MUFL, OT), and *traffic* (target: junction1, control: junction2, junction3). Metrics include RMSE, MASE, WQL, and average rank (lower is better). **Bold** highlights the best result within each row group; **bold+underlined** the overall best.

		bikesharing			eth1			traffic		
		RMSE	MASE	WQL	RMSE	MASE	WQL	RMSE	MASE	WQL
0-shot		0.728	2.150	0.287	0.678	2.132	0.255	0.708	1.555	0.255
Original Data (OD)		0.495	0.822	0.178	0.658	1.820	0.232	0.702	1.995	0.283
GEN	SDF-FPC ₃	0.527	0.926	0.200	0.692	1.914	0.246	0.699	2.029	0.287
	SDF-FPC ₅	0.530	0.918	0.198	0.693	2.003	0.252	0.662	1.837	0.262
	SDF-FPC ₇	0.522	0.915	0.197	0.650	1.887	0.232	0.812	2.265	0.323
	SDF-ICA ₃	0.514	0.899	0.194	0.647	1.829	0.233	0.730	2.068	0.294
	SDF-ICA ₅	0.537	0.909	0.194	0.637	1.934	0.233	0.655	1.849	0.262
	SDF-ICA ₇	0.517	0.898	0.193	0.626	1.820	0.224	0.790	2.189	0.312
OG + GEN	SDF-FPC ₃ + OD	0.493	0.829	0.179	0.658	1.780	0.229	0.736	2.077	0.296
	SDF-FPC ₅ + OD	0.487	0.807	0.174	0.659	1.757	0.230	0.743	2.087	0.297
	SDF-FPC ₇ + OD	0.492	0.821	0.177	0.666	1.754	0.231	0.706	1.993	0.283
	SDF-ICA ₃ + OD	0.487	0.801	0.173	0.640	1.790	0.228	0.734	2.074	0.295
	SDF-ICA ₅ + OD	0.486	0.804	0.174	0.649	1.780	0.230	0.750	2.110	0.301
	SDF-ICA ₇ + OD	0.490	0.810	0.175	0.642	1.746	0.226	0.718	2.025	0.288

Table D.8: Average Generation Time Across LLM Backbones. Average time (in seconds) required to generate synthetic univariate time series for the *bikesharing* dataset across three targets: count, temperature, and humidity. We report results for two input sequence lengths (250 and 500) and compare three LLM backbones: GPT-2, granite-3.0-2b-base, and Phi-3.5-mini-instruct. All models were evaluated under the same computational constraints (-mem 100G -cores 1+1 -gpu a100) using a single NVIDIA A100 GPU. For fine-tuning, we use a batch size of 16 for granite and 8 for phi.

Length	ICA ₃ + gpt2	ICA ₃ + granite	ICA ₃ + phi	ICA ₅ + gpt2	ICA ₅ + granite	ICA ₅ + phi	ICA ₇ + gpt2	ICA ₇ + granite	ICA ₇ + phi
250	22.7	112.8	132.6	18.3	118.5	113.9	19.0	119.9	126.1
500	16.2	93.6	98.5	17.3	99.9	103.7	18.9	125.0	110.7

Table D.9: Ablation study: LLM backbone. Aggregated similarity-based performance across all datasets for different LLMs used in SDF models. We compare GPT-2 with two larger and more recent alternatives: granite-3.0-2b-base⁷ (2B parameters) and Phi-3.5-mini-instruct⁸ (3.8B parameters). For fine-tuning, we use a batch size of 16 for granite and 8 for phi.

		Feature-based				Distance-based			Norm. Avg.	
		MDD	ACD	SD	KD	ED	DTW	SHR	Feat.	Dist.
MULTISAMPLE	SDF-FPC ₃ + GPT-2	0.255	2.166	1.323	4.299	17.749	11.921	16.537	0.964	0.747
	SDF-FPC ₃ + Granite	0.251	1.817	1.227	4.132	16.429	11.659	11.565	0.757	0.245
	SDF-FPC ₃ + Phi-3	0.257	1.215	1.154	3.723	16.734	11.872	12.367	0.643	0.397
	SDF-ICA ₃ + GPT-2	0.244	1.180	0.869	2.384	16.669	12.373	6.870	0.101	0.361
	SDF-ICA ₃ + Granite	0.241	1.069	0.961	2.524	16.953	12.744	6.160	0.101	0.509
	SDF-ICA ₃ + Phi-3	0.247	0.907	1.102	3.570	16.069	11.847	6.499	0.382	0.069
UNIVARIATE	SDF-FPC ₃ + GPT-2	0.308	1.480	0.801	1.690	19.340	12.809	5.452	0.947	0.804
	SDF-FPC ₃ + Granite	0.305	1.268	0.673	1.185	19.026	12.556	5.457	0.207	0.505
	SDF-FPC ₃ + Phi-3	0.310	1.368	0.671	1.305	19.561	12.767	5.196	0.574	0.777
	SDF-ICA ₃ + GPT-2	0.306	1.396	0.671	1.382	18.802	12.435	4.856	0.496	0.161
	SDF-ICA ₃ + Granite	0.304	1.370	0.679	1.123	18.616	12.365	4.712	0.253	0.000
	SDF-ICA ₃ + Phi-3	0.307	1.398	0.541	1.199	19.081	12.471	5.856	0.337	0.577

Table D.10: Multisample evaluation: similarity metrics reported per dataset.

		SDForger Models		VAE Models		GAN Models		Others
		ICA ₃	FPC ₃	TimeVAE	TimeVQVAE	RTSGAN	SDEGAN	LS4
ECL	MDD	0.154	0.219	0.156	0.292	0.145	0.193	0.296
	ACD	0.146	4.492	0.082	7.862	0.051	0.174	8.365
	SD	2.47	2.762	0.746	2.803	0.114	2.91	2.983
	KD	7.342	6.07	3.294	6.895	1.001	8.673	10.074
	ED	10.141	12.543	12.887	9.978	13.461	25.951	43.715
	DTW	9.715	10.985	12.025	7.97	12.486	25.431	40.142
	SHAP-RE	0.424	4.027	1.922	2.21	4.123	7.048	105.287
NNS	MDD	0.248	0.248	0.243	0.371	0.383	0.246	0.262
	ACD	1.489	3.235	0.221	4.964	4.646	2.73	5.677
	SD	0.307	0.428	0.126	0.259	0.092	0.422	0.287
	KD	1.43	4.249	0.151	1.159	0.348	0.512	0.96
	ED	19.308	20.576	20.514	15.019	16.201	43.433	38.822
	DTW	12.837	12.617	11.223	10.914	9.684	36.712	24.415
	SHAP-RE	9.482	40.975	20.993	2.072	8.254	83.918	207.419
Tourism	MDD	0.189	0.24	0.172	0.339	0.121	0.208	0.282
	ACD	0.22	3.29	0.206	7.807	0.272	0.215	8.228
	SD	1.321	2.613	0.854	2.896	0.681	2.988	2.806
	KD	4.477	8.297	4.251	7.877	4.852	9.616	10.907
	ED	11.216	14.039	13.895	10.516	15.405	25.399	39.897
	DTW	10.291	11.837	12.409	8.192	14.741	25.098	35.521
	SHAP-RE	0.547	4.28	1.785	2.135	2.833	6.409	100.231
Traffic	MDD	0.251	0.234	0.234	0.359	0.314	0.222	0.242
	ACD	1.443	1.368	0.097	3.767	0.886	3.749	5.229
	SD	1.433	1.507	0.353	1.377	1.384	1.598	1.403
	KD	3.177	1.937	1.263	1.503	2.642	3.113	4.727
	ED	16.532	18.429	20.748	14.169	15.552	35.522	55.908
	DTW	10.917	10.5	12.343	10.039	9.164	31.69	37.028
	SHAP-RE	6.568	9.188	14.948	1.995	5.101	51.49	205.07
Weather (Maxtemp)	MDD	0.292	0.293	0.282	0.447	0.303	0.286	0.296
	ACD	1.097	2.221	0.533	6.717	1.15	0.705	7.597
	SD	0.131	0.017	0.435	0.005	0.37	0.237	0.142
	KD	0.419	2.561	0.591	2.188	0.584	0.527	0.976
	ED	25.51	21.661	19.665	15.113	19.77	43.035	46.189
	DTW	20.532	15.354	13.238	11.219	15.884	41.331	34.55
	SHAP-RE	6.638	24.439	9.079	2.098	3.931	34.196	152.274
Weather (Mintemp)	MDD	0.271	0.27	0.264	0.41	0.365	0.266	0.275
	ACD	1.705	1.053	0.278	5.937	1.508	1.67	6.737
	SD	0.185	0.216	0.304	0.05	0.398	0.249	0.145
	KD	1.065	1.789	0.757	1.936	0.985	0.213	1.174
	ED	17.199	18.533	19.575	15.177	15.575	44.094	46.266
	DTW	13.148	11.255	10.48	10.675	10.837	41.651	32.415
	SHAP-RE	6.217	14.613	15.605	1.956	2.587	55.846	208.289
Weather (Rain)	MDD	0.233	0.222	0.175	0.291	0.259	0.199	0.27
	ACD	1.642	0.321	0.309	2.491	2.735	5.549	4.696
	SD	0.599	2.474	1.065	2.683	1.641	2.729	2.135
	KD	1.146	6.636	3.238	7.94	7.447	9.639	9.724
	ED	14.461	16.009	16.979	13.631	15.033	31.412	50.966
	DTW	10.935	11.493	11.35	10.718	10.803	28.891	33.017
	SHAP-RE	10.955	9.555	25.464	1.883	9.595	57.118	224.024
Weather (Solar)	MDD	0.314	0.31	0.29	0.459	0.342	0.297	0.284
	ACD	1.695	1.351	0.349	4.18	2.902	1.996	2.667
	SD	0.508	0.564	0.172	0.539	0.216	0.101	0.044
	KD	0.013	2.854	0.029	1.618	0.544	0.433	0.27
	ED	18.989	20.201	20.061	15.69	17.677	48.549	33.346
	DTW	10.61	11.322	9.932	11.607	11.275	36.321	17.363
	SHAP-RE	14.132	25.218	22.375	1.892	8.623	117.395	80.632

⁷<https://huggingface.co/ibm-granite/granite-3.0-2b-base>

⁸<https://huggingface.co/microsoft/Phi-3.5-mini-instruct>

Table D.11: Univariate evaluation: similarity metrics reported for Energy datasets.

		SDForger Models		VAE Models		GAN Models		Others
		ICA ₃	FPC ₃	TimeVAE	TimeVQVAE	RTSGAN	SDEGAN	LS4
Appliances	MDD	0.318	0.315	0.303	0.405	0.414	0.241	0.251
	ACD	1.825	1.714	3.137	1.714	2.404	7.208	4.301
	SD	2.068	2.093	1.008	2.07	2.152	2.269	2.028
	KD	3.249	3.816	2.891	2.586	2.559	4.196	5.874
	ED	19.493	19.13	20.459	15.916	17.162	29.562	47.81
	DTW	11.597	11.73	10.03	12.322	11.301	27.191	16.564
	SHAP-RE	9.588	9.072	27.262	1.952	6.367	71.477	162.749
Australian Elec (T000000)	MDD	0.315	0.312	0.292	0.457	0.376	0.281	0.323
	ACD	1.069	0.392	1.431	5.641	1.926	2.976	7.129
	SD	0.165	0.103	0.65	0.071	0.3	0.091	0.423
	KD	0.161	0.452	1.296	2.12	1.829	0.325	0.765
	ED	19.017	22.663	19.656	15.657	22.511	42.67	38.681
	DTW	10.652	13.655	10.899	10.583	14.942	40.842	26.104
	SHAP-RE	3.411	2.719	7.925	2.441	4.007	23.325	34.777
Australian Elec (T000001)	MDD	0.287	0.281	0.277	0.436	0.421	0.273	0.293
	ACD	1.46	0.457	0.265	5.579	4.796	2.518	6.908
	SD	0.274	0.307	0.11	0.137	0.589	0.031	0.032
	KD	1.8	1.677	0.503	1.99	0.264	0.273	0.899
	ED	18.368	19.769	19.51	15.717	20.145	44.034	37.357
	DTW	12.248	12.842	10.312	10.648	13.322	41.201	25.029
	SHAP-RE	2.211	2.91	6.061	2.587	3.291	26.765	30.768
Australian Elec (T000002)	MDD	0.313	0.313	0.292	0.486	0.334	0.297	0.315
	ACD	1.196	0.569	0.237	5.675	2.541	2.559	7.209
	SD	0.42	0.718	0.322	0.598	0.605	0.387	0.229
	KD	0.179	0.69	0.539	2.111	2.386	0.389	0.804
	ED	20.624	21.174	19.537	15.889	19.896	45.934	37.731
	DTW	13.17	13.104	10.626	10.748	14.559	44.425	26.567
	SHAP-RE	2.683	3.04	4.984	2.38	1.572	23.29	28.057
Australian Elec (T000003)	MDD	0.283	0.289	0.279	0.444	0.41	0.261	0.286
	ACD	1.549	1.35	0.455	5.174	4.187	2.791	6.412
	SD	0.399	0.389	0.135	0.221	0.822	0.365	0.034
	KD	0.057	0.465	0.226	1.596	0.524	0.127	1.343
	ED	17.406	19.377	20.146	15.975	18.751	40.657	40.4
	DTW	11.621	14.456	11.466	11.025	11.502	37.719	28.914
	SHAP-RE	1.888	1.929	4.942	2.522	3.095	17.34	26.566
Australian Elec (T000004)	MDD	0.293	0.287	0.28	0.458	0.337	0.277	0.302
	ACD	1.68	0.887	1.735	4.565	2.658	3.209	6.726
	SD	0.088	0.062	0.666	0.136	0.173	0.057	0.365
	KD	0.199	0.664	1.679	2.199	0.691	0.527	0.706
	ED	19.85	19.864	20.51	15.88	19.327	44.238	41.623
	DTW	11.8	12.582	10.921	10.933	12.972	40.349	28.13
	SHAP-RE	4.11	4.468	11.67	2.523	4.131	39.504	54.245
ETTH1 (HUFL)	MDD	0.326	0.32	0.29	0.476	0.381	0.291	0.326
	ACD	1.249	1.376	3.618	2.678	4.233	4.542	4.778
	SD	0.355	0.45	0.956	0.371	0.153	0.142	0.751
	KD	0.745	0.845	1.5	2.067	0.869	1.0	0.276
	ED	19.324	20.103	21.804	16.021	17.323	45.316	25.175
	DTW	9.475	9.579	10.69	11.35	10.616	38.346	9.745
	SHAP-RE	9.878	13.289	28.806	1.94	7.684	129.161	48.028
ETTH1 (OT)	MDD	0.235	0.24	0.225	0.354	0.268	0.254	0.272
	ACD	2.276	1.163	1.923	4.969	2.67	3.337	6.463
	SD	0.104	0.179	1.006	0.332	0.76	0.176	0.134
	KD	0.892	0.097	0.651	1.089	0.936	0.645	1.885
	ED	20.481	18.292	22.676	15.583	20.463	51.747	42.246
	DTW	12.525	12.195	12.614	10.499	11.718	49.511	25.674
	SHAP-RE	3.368	3.444	15.306	2.174	5.613	52.871	52.186

Table D.12: Univariate evaluation: similarity metrics reported for Transport datasets.

		SDForger Models		VAE Models		GAN Models		Others
		ICA ₃	FPC ₃	TimeVAE	TimeVQVAE	RTSGAN	SDEGAN	LS4
Bikesharing (Count)	MDD	0.326	0.336	0.295	0.492	0.444	0.29	0.332
	ACD	0.856	0.691	2.493	1.712	2.451	4.306	1.972
	SD	0.101	0.12	0.202	0.042	0.251	0.61	0.035
	KD	0.571	0.258	0.125	1.447	0.091	0.218	0.387
	ED	21.389	19.406	21.314	16.172	19.806	44.217	21.848
	DTW	10.305	10.036	10.163	12.804	10.225	31.743	10.347
	SHAP-RE	13.665	13.77	38.651	2.012	19.352	247.88	64.166
Bikesharing (Humidity)	MDD	0.318	0.322	0.301	0.432	0.365	0.266	0.289
	ACD	1.653	1.94	4.68	2.715	3.323	4.948	3.845
	SD	0.116	0.113	0.569	0.076	0.367	0.425	0.617
	KD	0.521	0.806	0.671	1.831	0.511	0.404	1.13
	ED	19.761	18.098	25.8	16.097	18.478	44.641	51.221
	DTW	10.699	10.847	13.416	10.907	10.25	36.872	26.846
	SHAP-RE	4.249	4.63	43.651	2.154	7.005	88.647	100.497
Bikesharing (Temperature)	MDD	0.37	0.372	0.363	0.451	0.386	0.291	0.339
	ACD	1.426	1.662	0.086	5.766	2.137	1.244	7.736
	SD	0.13	0.488	0.43	0.534	0.808	0.11	0.53
	KD	1.91	0.931	0.536	1.776	1.228	0.409	1.334
	ED	17.172	20.38	19.349	15.702	20.591	49.379	39.062
	DTW	12.107	12.47	11.074	10.569	15.251	46.37	26.093
	SHAP-RE	2.807	4.426	7.514	2.189	6.538	42.472	50.348
Traffic (Junction 1)	MDD	0.3	0.294	0.277	0.42	0.403	0.267	0.313
	ACD	0.924	0.861	4.631	2.642	2.195	6.292	3.854
	SD	0.276	0.018	0.667	0.008	0.225	0.167	0.266
	KD	3.793	2.151	0.769	1.807	0.317	0.052	1.168
	ED	18.191	18.465	25.655	15.782	16.151	45.765	36.403
	DTW	10.776	10.597	13.931	10.893	10.065	41.767	18.485
	SHAP-RE	5.198	5.21	31.453	2.124	4.393	82.871	58.632
Traffic (Junction 2)	MDD	0.367	0.368	0.352	0.434	0.445	0.281	0.315
	ACD	2.893	2.265	2.889	2.878	2.516	5.164	4.492
	SD	0.272	0.237	0.526	0.086	0.992	0.328	0.295
	KD	1.212	0.645	1.135	1.921	2.667	0.273	1.155
	ED	17.937	18.765	21.622	16.007	17.114	44.67	41.478
	DTW	10.246	10.425	10.307	10.995	11.314	38.389	19.57
	SHAP-RE	5.546	6.777	30.016	2.157	3.426	135.497	99.919
Traffic (Junction 3)	MDD	0.326	0.326	0.326	0.41	0.361	0.25	0.276
	ACD	2.788	2.444	3.861	2.123	3.308	5.97	4.377
	SD	0.898	1.039	0.054	0.906	0.23	1.056	1.257
	KD	1.086	0.684	0.262	0.336	0.776	1.283	2.822
	ED	17.961	18.412	22.054	16.058	18.829	38.533	53.251
	DTW	11.558	11.147	10.892	11.807	10.677	32.538	25.618
	SHAP-RE	6.848	7.446	46.675	2.022	12.436	118.245	178.736

Table D.13: Univariate evaluation: similarity metrics reported for Nature datasets.

		SDForger Models		VAE Models		GAN Models		Others
		ICA ₃	FPC ₃	TimeVAE	TimeVQVAE	RTSGAN	SDEGAN	LS4
CCP (CO2)	MDD	0.173	0.186	0.166	0.3	0.179	0.232	0.236
	ACD	1.391	1.119	2.203	5.536	2.598	3.06	6.866
	SD	0.472	2.21	2.481	1.984	1.12	1.809	1.86
	KD	1.644	3.443	4.155	3.31	3.72	5.09	6.164
	ED	18.442	18.729	26.232	14.19	14.734	72.136	36.803
	DTW	15.245	14.344	18.308	10.176	10.831	71.196	28.544
	SHAP-RE	1.123	1.684	13.719	2.486	1.329	52.729	25.99
CCP (NH3)	MDD	0.452	0.477	0.409	0.67	0.392	0.364	0.455
	ACD	0.312	2.223	0.55	6.779	0.56	0.822	9.168
	SD	0.416	0.766	0.272	0.441	0.23	0.346	0.753
	KD	1.267	0.554	0.212	0.292	0.671	0.011	2.743
	ED	16.965	19.28	17.18	15.465	22.525	31.041	35.404
	DTW	15.495	17.18	14.483	12.381	19.973	30.589	29.251
	SHAP-RE	0.423	1.064	1.13	2.418	2.904	2.805	9.832
CCP (C4H11NO)	MDD	0.197	0.191	0.158	0.266	0.189	0.189	0.229
	ACD	0.662	0.822	0.152	6.672	0.371	0.231	8.524
	SD	1.747	2.232	0.007	2.294	0.626	2.729	2.511
	KD	2.054	3.638	3.105	4.998	0.251	6.454	8.179
	ED	15.92	16.128	15.448	11.295	14.54	38.679	49.348
	DTW	12.168	11.741	10.881	8.252	10.213	37.706	40.586
	SHAP-RE	1.255	2.426	2.801	2.363	2.042	14.476	47.176
CCP (C4H10N2)	MDD	0.178	0.18	0.162	0.249	0.221	0.19	0.249
	ACD	1.514	1.273	0.535	4.522	2.445	3.142	5.538
	SD	1.675	1.638	0.512	1.456	1.398	1.831	1.659
	KD	0.157	2.451	0.824	3.091	4.551	4.592	6.204
	ED	15.698	17.378	19.159	13.879	21.6	46.177	45.823
	DTW	11.646	12.004	12.098	10.002	14.647	44.366	33.614
	SHAP-RE	2.299	4.547	6.142	2.228	5.582	31.911	59.928

Table D.14: Univariate evaluation: similarity metrics reported for Finance datasets.

		SDForger Models		VAE Models		GAN Models		Others
		ICA ₃	FPC ₃	TimeVAE	TimeVQVAE	RTSGAN	SDEGAN	LS4
Exchange Rate (Currency 1)	MDD	0.27	0.269	0.267	0.415	0.358	0.278	0.308
	ACD	0.851	1.727	0.211	7.212	1.062	0.932	8.803
	SD	0.409	0.62	0.33	0.614	1.031	0.476	0.332
	KD	0.32	1.173	0.058	1.77	0.854	0.034	1.275
	ED	18.913	19.909	20.652	15.335	26.589	47.853	35.288
	DTW	15.572	15.91	16.319	11.256	22.394	46.856	26.695
	SHAP-RE	1.759	2.228	2.32	2.449	5.691	17.248	22.698
Exchange Rate (Currency 2)	MDD	0.316	0.303	0.286	0.459	0.343	0.253	0.291
	ACD	0.426	1.424	0.305	7.14	0.983	0.976	8.597
	SD	1.285	0.914	0.289	0.863	0.424	1.034	1.083
	KD	2.003	1.249	1.507	1.576	0.443	0.208	1.636
	ED	17.727	19.579	18.253	14.43	18.272	32.215	45.617
	DTW	15.12	16.076	14.15	10.689	14.488	31.633	38.042
	SHAP-RE	0.967	1.186	1.744	2.442	2.217	6.681	28.819
Exchange Rate (Currency 3)	MDD	0.369	0.428	0.36	0.614	0.47	0.314	0.348
	ACD	0.113	2.852	0.157	8.035	0.639	0.106	9.934
	SD	0.22	0.751	0.122	0.453	1.154	0.633	0.71
	KD	0.64	3.039	0.205	2.755	0.046	0.992	0.369
	ED	19.578	21.042	19.31	14.765	21.985	28.394	38.289
	DTW	19.092	19.25	18.532	12.47	20.528	28.143	34.966
	SHAP-RE	0.485	0.956	0.808	2.44	1.168	2.133	15.265
Exchange Rate (Currency 4)	MDD	0.342	0.341	0.341	0.543	0.349	0.279	0.317
	ACD	0.34	1.427	0.848	7.171	1.132	1.023	8.913
	SD	0.647	0.252	0.136	0.349	0.49	0.502	0.686
	KD	0.484	1.206	0.69	2.483	0.394	0.666	0.645
	ED	20.09	20.287	19.622	15.38	20.51	33.675	42.123
	DTW	16.021	16.187	13.507	10.985	14.745	32.558	33.075
	SHAP-RE	1.18	1.383	1.85	2.34	1.858	7.303	23.273
Exchange Rate (Currency 6)	MDD	0.273	0.28	0.251	0.427	0.338	0.237	0.286
	ACD	0.204	1.893	0.179	7.773	0.578	0.414	8.341
	SD	0.285	0.755	0.245	0.342	0.049	0.481	0.464
	KD	0.534	3.95	0.88	1.701	1.127	0.152	1.401
	ED	19.809	19.763	16.956	14.579	21.034	39.025	34.643
	DTW	18.469	17.954	14.799	11.822	18.02	38.671	30.317
	SHAP-RE	0.569	0.82	1.036	2.386	2.427	5.158	28.882
Exchange Rate (Currency 7)	MDD	0.318	0.353	0.322	0.493	0.374	0.292	0.334
	ACD	0.17	2.423	0.179	7.967	0.121	0.22	9.778
	SD	0.249	0.169	0.212	0.22	0.61	0.344	0.599
	KD	0.743	3.389	0.574	2.616	0.379	0.759	0.443
	ED	19.565	23.189	15.034	14.768	21.199	36.463	34.437
	DTW	18.484	20.773	13.105	12.875	19.659	36.214	30.555
	SHAP-RE	0.945	0.761	0.981	2.496	0.918	2.649	9.963
Exchange Rate (Currency 8)	MDD	0.401	0.378	0.358	0.564	0.467	0.339	0.353
	ACD	0.06	2.259	0.119	8.052	0.197	0.077	10.102
	SD	0.091	0.04	0.595	0.173	0.253	0.041	0.333
	KD	1.009	2.867	0.716	2.751	0.202	0.891	0.205
	ED	16.88	21.571	16.902	14.882	21.432	37.487	42.048
	DTW	16.254	20.245	15.651	12.884	20.061	37.232	39.402
	SHAP-RE	0.232	1.044	0.638	2.43	0.679	3.228	15.895